Residual Structure and Mechanical Properties of Alpha Brass and Stainless Steel Following Deformation by Cold Rolling and Explosive Shock Loading

L. E. Murr and F. I. Grace

N69-75804

Abstract

The mechanical responses and residual defect structures in 70/30 brass and type 304 stainless steel following explosive shock loading and cold reduction by rolling have been studied. A distinct relationship was observed to exist between the residual mechanical properties and microstructures observed by transmission electron microscopy. Shock-loaded brass deformed primarily by the formation of coplanar arrays of dislocations and stacking faults at lower pressures, and twin-faults (deformation twins and ε - martensite bundles) at higher pressures (> 200 Kb). The microstructures of cold-rolled brass were characterized by dense dislocation fields elongated in the rolling direction. Stainless steel was observed to deform by the formation of dense arrays of stacking faults at lower shock pressures and twin-faults at high shock pressures (> 200 Kb). Lightly cold-rolled

---

L. E. Murr, Member AIME, is Assistant Professor of Materials Science and Electrical Engineering, University of Southern California, Los Angeles, California.

F. I. Grace is Research Physicist, Materials Science Division, Naval Weapons Laboratory, Dahlgren, Virginia.

stainless steel deformed similar to low pressure shock-loaded stainless steel, but transformed to α'-martensite in heavily cold-rolled stainless steel. Discontinuous yielding was observed for the heavily cold-rolled stainless steel, and stress relaxation in the pre-yield region for cold-rolled and shock-loaded stainless steel was interpreted as an indication of the ability of twin-faults and stacking faults to act as effective barriers to dislocation motion. A simple model for the formation of the planar defects and α' martensite is presented based on the propagating of Shockley partial and half-partial dislocations.

INTRODUCTION

A considerable effort has been expended over the past decade in an attempt to elucidate the response of metallic-crystalline solids to the passage of a high velocity shock wave (e.g., Smith[1]; Dieter[2]; and Zukas[3]). While it has been possible to obtain relevant information pertaining to the residual defect structures and mechanical properties, there have been few rigorous attempts to draw a direct comparison between these structures and properties. In addition, numerous investigators have recently observed the occurrence of deformation twinning in shock deformed fcc metals (e.g., Nolder and Thomas[4], and Johari and Thomas[5]), but little attempt has been made to elucidate the mechanisms of formation of these defects. Comparative data for metals deformed by shock-loading and the same metals deformed by more conventional modes of deformation such as cold-reduction by rolling is also generally lacking. The present investigation therefore has the following objectives: (1) to examine the mechanical properties of some explosively shock loaded and cold-rolled fcc metals of low stacking-fault energy as a function of their residual substructures; (2) to present a simple model for the formation twin-faults and related defect structures in the low stacking-fault energy materials of interest (70/30 brass, $\gamma_{SF} \cong 14$ ergs/cm^2; and 304 stainless steel, $\gamma_{SF} \cong 21$ ergs/cm^2); (3) to make some deductions with regard to the residual characteristics of dislocation and planar defect substructures in cold rolled and shock loaded 70/30 brass and type 304 stainless steel. In particular, it was desirable to characterize the residual hardening effects of particular deformation substructures.

I) EXPERIMENTAL PROCEDURE

Sheet samples of 70/30 brass (.005 and .15 in. thick; annealed at 659°C for 2 hrs.) and type 304 stainless steel (.007 in. thick; annealed 0.25 hr. at 1060°C) of nominal compositions shown in Table 1 were cold-rolled in one direction only to produce reductions in thickness of 15%, 30%, 45%, 60%, and 75% in the brass; and 5%, 15%, 25%, 35% and 45% in the stainless steel. Identical sheet samples in the annealed (unrolled) state were subjected to plane compressive shock waves to various peak pressures ranging from 0-400 Kb in the brass and 0-425 Kb in the stainless steel; and with a constant peak pressure duration of approximately 2 microseconds. A detailed description of the shock loading technique has been given previously[6].

Tensile specimens 1.0 in. in length and 0.125 in. in width were cut from the cold-rolled sheets (tensile axis parallel to the rolling direction), and the shock-loaded sheet specimens. Stress (load)-strain (elongation) measurements on the tensile specimens were made on a Tinius-Olsen load-compensating tensile tester using a strain rate of 2.7×10^{-3} sec.$^{-1}$. Tensile tests were repeated at least twice, giving essentially the same results. Stress relaxation measurements in the pre-yield region were also made using an initial strain rate of 5.4×10^{-4} sec^{-1}.

In addition to tensile and stress relaxation measurements, Vickers microhardness measurements were made on all samples. A total of 100 microhardness readings were obtained for each specimen following a light electropolish to ensure uniform surface conditions for all tests. The hardness averages obtained generally carried a 96 percent confidence limit of ± 3 points.

Thin foils for transmission electron microscopy studies were prepared from the brass and stainless steel specimens as described previously by Grace, et al[7] and Murr[8] respectively. Electron microscope observations were made at an accelerating potential of 100 kV using a goniometer tilt stage.

II) EXPERIMENTAL RESULTS

Because of the fact that the foil specimen surface planes in both the shock-loaded and the cold-rolled materials were normal to the explosively initiated shock wave in one case, and the roll pressure direction in the other; there exists a certain uniqueness in comparing these distinct deformation modes. On the other hand, shock-loading represents a high rate plane strain process in contrast to a low rate triaxial strain situation characterizing cold-reduction by rolling.

Residual Deformation Microstructures and Mechanical Properties for Shock-Loaded 70/30 Brass

Figures 1 and 2 illustrate "typical" substructures of explosively shock loaded brass. Unambiguous proof for twin-type deformation structures in brass foils shock-loaded to 200 kilobars and greater was also obtained using aperture dark-field techniques. Figure 3 shows typical stress-elongation curves for shock-loaded 70/30 brass tested at room temperature. The transmission electron micrographs (Figs. 1 and 2) illustrate that brass initially deforms by the creation of dense coplanar dislocation arrays, which eventually develop imperfect microtwins. These planar defects, initially developing as single stacking faults on (111) planes, become imperfect

twin structures at pressures above about 200 Kb, i.e., microtwins and interspersed ε - martensite (hcp stacking-fault bundles).

As a means to directly relate changes in substructural defect features with variations in the mechanical properties of the shock-loaded specimens, both the dislocation density and the twin-fault density (volume percent) were estimated at the various shock pressures from electron microscope images similar to and including those illustrated in Figs. 1 and 2. These data, essentially identical to that previously reported by Grace, et al[7], are reproduced for reference and comparison in Table 2. It is apparent from Table 2, and with reference to Figs. 1-3, that work-hardening and/or strengthening in shock-loaded brass is primarily the result of residual dislocations in the pressure range 0-200 Kb, whereas beyond 300 Kb peak pressure, the formation of twin-type defects might be assumed to contribute increasingly to the structural strengthening which occurs due to the impedance they offer to dislocation motion.

Residual Deformation Microstructures and Mechanical Properties for Cold-Rolled 70/30 Brass

Figures 4 and 5 show "typical" substructures associated with the various degrees of cold work in 70/30 brass, while Fig. 6 reproduces the associated stress-elongation curves for the same brass (tested at room temperature). Similar microstructures and mechanical properties associated with brass shock-loaded to 200 Kb and cold-rolled to about 30% reduction in thickness is apparent. Beyond these limits, the structural properties vary considerably, with the basic mode of deformation in cold-worked brass

being the densification of dislocations in elongated "fields" presumably influenced by the rolling direction (although this point has not been unambiguously proven). The appearance of twin-type structures at 60% and 75% reduction (Fig. 5b), although prevalent in numerous grains, was not observed to occupy more than 1% of the total volume of the material (at 75% reduction). It is apparent that the twin-mode originates at higher degrees of cold work as an accommodation mechanism to relieve the shear developed in the elongated dislocation fields. In this respect, it is interesting to note the high degree of perfection (i.e., sharpness of texture) maintained by the dense dislocation fields. (Fig. 5a inset selected-area electron diffraction pattern). This feature is perhaps significant evidence of the general absence of mechanical twins or twin-faults as well as the absence of disrupted grain boundaries at these more advanced stages of cold work. Figure 6 might be interpreted to illustrate that, with reference to Fig. 3, the behavior of the residual substructures for brass shock-loaded at high pressures and rolled to highly cold-worked states is effectively similar. It is therefore apparent that the twin-faults, presumably interspersed in dense dislocation arrangements in highly shocked brass, exhibit the same basic impedance response to dislocation motion as the dense, elongated dislocation "fields" in the severely cold-rolled brass.

The measurement of dislocation densities in the cold-rolled brass produced estimates differing significantly from those obtained for the shock-loaded material at higher pressures. These estimates, along with the respective Vickers microhardness averages, are listed in Table 3. Owing

to the strain contrast effects arising in foils with a large concentration of dislocations, sensible estimates could not be reliably made for brass cold rolled in excess of 60% reduction in thickness.

Residual Deformation Microstructures and Mechanical Properties for Shock-Loaded 304 Stainless Steel

Microstructures observed for shock-loaded stainless steel were similar, in only a few respects, to those observed for brass at low shock pressures. While stainless steel did possess abundant coplanar dislocation arrays at 120 Kb, stacking faults appeared as the prominent substructural feature. These faults densified and extended more liberally with increasing pressure than in brass. The formation of twin-faults at higher pressures in stainless steel was significantly greater than observations for brass at essentially concurrent peak pressures as illustrated in Fig. 7. Typical stress-elongation curves for stainless steel, tested at room temperature after the various shock-loading treatments, are shown in Fig. 8.

Because of the predominance of twin-faults in the residual substructure in shock-loaded stainless steel, and associated contrast effects at dislocation strain fields, some difficulties were experienced in measuring dislocation densities in the deformed stainless steel. The values recorded in Table 4 should therefore be considered as essentially relative magnitudes.

Estimates of the twin-fault densities, assuming the thickness to average 10 Å for 120 and 145 Kb samples and 150 Å for shock pressures in the range 235-425 Kb; and corresponding microhardness as previously reported

by Inman, et al[9] are reproduced in Table 4 for purposes of reference and comparison. It is observed from Table 4, and with reference to Figs. 7 and 8, that the production and propagation of stacking faults and twin-faults represents a significant contribution to work-hardening in shock-loaded stainless steel.

Residual Deformation Microstructures and Mechanical Properties for Cold-Rolled 304 Stainless Steel

As shown in the electron micrographs reproduced in Figs. 9 and 10, the terminal substructure for highly cold-worked stainless steel differs significantly from that observed for shock-loaded stainless steel; and shock-loaded and cold-rolled brass. The prominent feature of the stainless steel cold-worked substructures in the occurrence of a hexagonal close-packed phase (ε) at thickness reductions greater than about 10% and an associated formation of various volume percents of bcc (α') martensite which then increases with an increase in the percent of cold reduction. Direct observations of martensitic (α') platelets allowed a direct estimate of their volume percent in the originally fcc austenite (γ) matrix by measuring the total martensite platelet area per unit grain area, (e.g., Fig. 10) and simply equating the ratio α'/γ as a volume percentage. The results of electron transmission image measurements of α' volume densities are listed in Table 5. Table 5 also lists, for comparison, the average microhardness values measured for the cold-rolled stainless steel samples, and dislocation densities.

Figure 11 shows typical stress-elongation curves for 304 stainless steel cold-rolled as specified (tested at room temperature). As might be

expected from the great divergence in the substructures on comparing the cold-rolled stainless steel specimens with those shock-loaded, the tensile properties shown in Fig. 11 differ markedly from those observed in Fig. 8; and exhibit discontinuous yield phenomena in the elastic and plastic responses as the martensite density increases with the degree of cold work.

Stress Relaxation in Cold-Rolled and Shock-Loaded Stainless Steel

Discontinuous yielding observed for severely cold-rolled stainless steel (Fig. 11) can be phenomenologically interpreted as a locking and unlocking of dislocations from pinning points. As a means to more fully elucidate this occurrence, and to differentiate the "locking" ability of martensite in the cold-rolled stainless steel compared with the deformation twins in the shock-loaded stainless steel, stress relaxation measurements were conducted on these materials.

As a simple means to relate plastic strain rate to an average dislocation velocity, we write

$$\frac{d\epsilon}{dt} = \frac{b \Lambda v}{2} \quad , \qquad [1]$$

where ϵ is the strain, b is the dislocation Burgers vector (2.52 Å in 304 stainless steel), Λ is the density of mobile dislocations; and v is the average dislocation velocity. Several investigators (e.g. Thornton and Hirsch[10] and Bodner[11]) have considered the dislocation velocity to be a function of the shear stress excess over the back stress opposing dislocation motion

(resolved in the slip direction). Thus, the stress increment needed to maintain a particular dislocation velocity is essentially equal to the increment in the back stress, τ_B, due to strain hardening. For an applied shear stress, τ, we can write

$$v = \zeta (\tau - \tau)^m \qquad [2]$$

and

$$kT \ell n (v_o/v) = U_o - V_A (\tau - \tau_B) ; \qquad [3]$$

where ζ, v_o, and m are material constants, U_o is the energy supplied by the line tension in moving a dislocation jog without thermal activation, and V_A is the activation volume. The product, kT, is of course the Boltzmann constant multiplied by the absolute temperature. We can replace the shear stresses in Eqs. [2] and [3] above with the corresponding tensile stresses by considering[12]

$$(\tau - \tau_B) \cong .4 (\sigma - \sigma_B) , \qquad [4]$$

where σ is an applied tensile stress, and σ_B is the back stress.

The principal features of stress relaxation are that for constant strain, any relaxation of the initial stress must be due to dislocation motion or rearrangement. Relaxation in the pre-yield region can then be interpreted as a measure of the ability of deformation substructures (including dislocations, precipitates, twins, point defects, etc.) to act as barriers to the movement of free dislocations.

A number of the shock-loaded and cold-rolled stainless steel specimens were allowed to relax from some initial value, σ_o, to some lower value, σ_t, over a period of 5 min. Figure 12 illustrates the results for stainless steel cold-rolled (25%) and shock-loaded (425 Kb) to essentially the same hardness

(from Tables 4 and 5), and allowed to relax from a constant stress stop, σ_o, of approximately 92 Kpsi at room temperature. It is immediately apparent from Fig. 12 that the relaxation stress, $\Delta\sigma = (\sigma_o - \sigma_t)$, was twice as great for the cold-rolled material. It was also observed that $\Delta\sigma$ increased for each material tested as σ_o was increased, while maintaining the initial loading-rate constant.

By plotting the stress relaxation data as a function of the logarithm ($\log_{10}$) of the relaxation time, straight lines are produced whereby the material constants, m and V_A of Eqs. [2] and [3] may be evaluated from the slopes, S, of these curves[12,13]; i.e.,

$$S = \frac{d(\Delta\sigma)}{d(\log_{10} t)} \quad , \qquad [5]$$

$$m = \frac{2.3\,\sigma_o + S}{S} \quad ; \qquad [6]$$

and finally

$$V_A \cong \frac{kT}{S} \quad . \qquad [7]$$

Figure 13 shows the results of a series of stress relaxation measurements for stopping stresses, σ_o, between 60 and 90 Kpsi. Relaxation for the undeformed (control) material is shown for comparison in Fig. 13 at a similar stopping stress which, as observed in Figs. 8 and 11, is in the plastic (post-yield) region. Similar measurements at the yield point ($\sigma_o \cong 40$ Kpsi), and below, indicated less relaxation (reduced slope, S). However, the corresponding values of m and V_A obtained from Eqs. [6] and [7] respectively were very similar.

Table 6 lists the calculated values of the dislocation velocity stress dependence parameter, m; and the activation volume, V_A, corresponding to the stress relaxation data of Fig. 13 at T = 300° K. It is observed in Table 6 that both m and V_A increase with a corresponding increase in residual hardness and specific substructural volume density (twin-faults or martensite) by comparison with the data of Tables 4 and 5.

Determination of the Stacking-fault Character in Shock-Loaded and Cold-Rolled Brass and Stainless Steel

Utilizing the dark-field technique described by Art, et al[14] as well as the more direct bright-field image technique recently described by Van Landuyt, et al[15], the stacking-fault nature in all deformed brass and stainless steel samples was observed to be intrinsic. These stacking faults are characterized by the removal of one atomic (111) layer by the propagation of an S-Shockley partial dislocation with a Burgers vector of the type a/6 <112>.

III) DISCUSSION

The results of this investigation clearly indicate a distinct relationship between the residual mechanical properties and substructures of cold-rolled and shock-loaded stainless steel and 70/30 brass. This is evidenced by comparing the data of Figs. 3, 6, 8 and 11 with the corresponding microstructures shown in Figs. 1, 2, 4, 5, 7, 9 and 10; and the characteristic parameters listed in Tables 2-5. The reader can readily show that smoothly varying curves result when comparing hardness with the mode and magnitude of deformation,

0.2% yield stress from the stress-strain curves, ultimate tensile stress, and other similar correlations.

It is of interest to compare the results obtained in the present work with those obtained for copper, nickel, and aluminum shock-loaded and cold-rolled in the work of Appleton and Waddington[16]. In the case of these metals, discontinuous yielding occurred primarily for shock-loading, while no discontinuous yielding occurred for the same materials following cold reduction. These authors conclude the discontinuous yielding suggests the production of residual microstructures in which dislocations are pinned. Discontinuous yielding phenomena during straining in tension is then the result of unlocking and repinning of dislocations during yield, and in the subsequent flow period characterizing plastic deformation.

Recent work by Murr and Foltz[17], Rose and Berger[18] and Grace[19] has revealed that the substructures of shock-loaded as well as cold-rolled nickel, and copper, are all essentially characterized by the formation of dislocation cells. Aluminum is observed to form well defined cells only after cold reduction, and dislocation tangle forests following shock-loading. The dislocation cell structures differ in shape, dislocation wall density, and dimensions depending upon the metal, and the mode of deformation, i.e., shock-loading or cold-rolling. In nickel, dislocation cells have been observed to decrease in size with an increase in shock pressure, but to remain fairly symmetrical in shape[17]. Cold-reduction of nickel, as well as aluminum and copper produces dislocation cell structures. Cell structures in aluminum are not recognizable following shock deformation, and the residual micro-

structure is composed primarily of dense dislocation tangles and high coincidence of loops. In shock-loaded copper and nickel, there is also considerable evidence for dislocation loops, with a high coincidence of these defects in the dislocation cell walls as evidenced directly by transmission electron microscopy[20].

It appears that in the high stacking-fault energy metals, e.g., aluminum ($\gamma_{SF} \cong 400$ ergs/cm^2), nickel ($\gamma_{SF} \cong 300$ ergs/cm^2), and copper ($\gamma_{SF} \cong 70$ ergs/cm^2), as investigated by Appleton and Waddington[16], the dominant residual defect microstructure is the formation of dislocation cells and dense dislocation loops following shock deformation. While similar dislocation cell structures are also produced during reduction by cold rolling (these structures also exhibiting some dislocation and point defect loops); the fact that discontinuous yield phenomena is not observed for the cold-rolled materials leads one to suspect that a higher coincidence of point defects must be associated with the residual microstructures of shock-loaded, high stacking-fault energy materials. By direct contrast, the present work on materials of low stacking-fault energy, i.e., brass and stainless steel, illustrates that for dominant residual microstructures consisting primarily of planar-type defects, e.g., stacking faults, twin-faults, or coplanar arrays of densily packed dislocations; discontinuous yielding phenomena does not occur. This feature may point out the scarcity of point defects or point defect clusters in shock-loaded materials of low stacking-fault energy.

The discontinuous yielding phenomena observed for cold-rolled stainless steel, suggests that the incoherent martensite-matrix interface acts as

a barrier to dislocation motion associated with yield and plastic flow by carbon segregation. The similarity of martensite platelets in this respect with dislocation cell structures in shock-loaded materials as pointed out by the associated discontinuous yielding feature is perhaps indicative of irregular pinning.

Since the extension of dislocations into partials bounding a stacking fault affects the cross-slip, glide , and climb of free dislocations, stacking faults function as effective barriers to dislocation motion. The creation of a twin interface as the regularity of stacking faults increases simply perpetuates this barrier; and with increasing twin-fault density, the effective number of barriers per unit volume of material increases. Figure 12 illustrates this feature very convincingly since the stress relaxation from nearly the same pre-yield stopping stress, σ_o, is about double for material cold-rolled 25% as compared with the shock-loaded material. The fact that both the hardness and dislocation densities are nearly equal (Tables 4 and 5) leaves only the relative densities of martensite, or twin-faults respectively, to account for the observed differences in $\Delta\sigma$. Thus, where we have concluded above that martensite functions basically as a subgrain barrier to dislocation motion, we are lead to conclude further that twin-faults perform a similar function. The increase in twin-fault density with shock-loading functions in a manner analogous to the normal refinement of grains. The results of Fig. 13 as recorded in Table 6 also attest to this conclusion. It is apparent, upon comparing Table 6 and the associated parameters of Tables 4 and 5, that activation volume, and the effective dislocation velocity parameter, increase

with increasing deformation for stainless steel. We assume these same features will be observed for 70/30 brass.

The fact that stacking faults and stacking-fault bundles (ε-phase) are common to early stages of deformation by cold-reduction and shock-loading suggests that a close connection exists between stacking faults, and the subsequent and final deformation substructures. Numerous suggestions to this effect have been made in the past, e.g., Kelly and Nutting[21] found an α' bcc structure in 18 Cr-8Ni steel with $(111)_M \parallel (110)$, and proposed that the α'-phase formed from the γ austenite by a shear on the $(121)_M$ plane in the [121] direction with a simultaneous expansion perpendicular to the $(121)_M$ plane. In this scheme, the first shear displaces the atoms to a position which differs by only $\frac{a}{12}$ $<112>$ from that of a stacking fault. Experimental observations of martensite nucleation by Dash and Brown[22] also suggest that the transformation (α') occurs by a shear on $(111)_A$ by dislocations with $\bar{b} = \frac{1}{12} \rightarrow \frac{1}{18} a <112>$. Earlier investigation by Lagneborg[23] also suggests the formation of bcc faults by dissociation of Shockley partials of the $\frac{a}{6} <112>$ type into half Shockley partials $\frac{a}{12} <112>$, and that the volumes at these partials supply martensite nucleation sites.

From the experimental evidence introduced in the present work, it is concluded that the formation of arrays of stacking faults in low stacking-fault energy materials is basic to the formation of terminal structures at high levels of plastic deformation.

There are basically two schemes by which twin-faults are presumably created. These include the pole mechanism as developed in some detail by

Venables[24], and the creation of large numbers of partials through classical dislocation pile-ups as suggested by Cohen and Weertman[25]. If the pole mechanism involves a time dependency, this mechanism might be less likely in shock-loading than cold-reduction.

Since it has been shown, in the case of both shock-loading and cold-reduction, that the stacking-fault character in stainless steel is intrinsic, and that the dislocation density, even after small deformation, is approximately greather than $10^9 cm^{-2}$, the conditions necessary for both hcp formation and twinning are essentially met. The apparent selection of the defect mode in shock-loading or cold-reduction would seem to be dependent upon the variation in the shear accomodation and the rapidity of this accommodation with the mode of deformation (strain-rate effects).

In view of the results of the present investigation, it appears as though strain rate is essentially a determining factor in the mode of residual defect production, in association with the shear accommodation. Thus, dislocations created in the shock front, are presumably split into partials of the $\frac{a}{6}\langle 112\rangle$ type. This process, as well as the propagation of the stacking faults throughout the grains, can occur in a microsecond interval. As the load is increased, a critical number of partials are propagated, and stacking-fault bundles (ε-martensite) and/or twins begin to form. This process might be expected to be somewhat random, and the resulting microtwins formed would of necessity be imperfect since the passage of an S-Shockley partial on every $\{111\}$ plane would probably be interrupted. In addition, stacking-fault bundles or ε-phase platelets can also form within or adjacent to deformation

twins. In some cases, it is difficult to distinguish one from the other, and the defects are best described as twin-faults.

In the case of cold-rolled stainless steel, considerably more complex shearing and shear accommodation is involved than for shock loading. It is basically a triaxial strain situation as compared with the plane strain case for shock-loading. As shown in the electron micrographs (Fig. 10a), the stacking faults initially formed are not nearly extended to the degree exhibited in shock-loaded material, and it is evident, therefore, that perhaps the mode of formation, and certainly the mode of propagation is different with respect to shock-loading. The intermediate substructures, characterized by ε - phase (hcp) formation and the onset of bcc α' (martensite), followed by a high density of α' martensite as a terminal substructure at large cold reductions, is suggestive of a basically similar process.

In Fig. 14 is shown a simple mechanism sequence by which the residual substructures can occur basically as a result of a single dislocation property; namely that of the production and propagation of partial and half-partial dislocations (in the final production of martensite). In Fig. 14 the upper sequence characterizes the formation of intrinsically faulted austensite (γ(F)) by the propagation of $\frac{a}{6}$ <112> partial dislocations, and the subsequent formation of microtwins as the density of partials is increased with increased shock pressure. The alternate sequence is characterized by the formation of ε from the γ (F) with increasing partial formation, and the $\frac{a}{12}$ < 112> type propagation as a means to accommodate the shear and compression of cold

reduction. This latter process is favorable in stainless steel because of interstitial carbon atoms in the lattice structure.

The general dislocation reaction scheme then appears as follows:

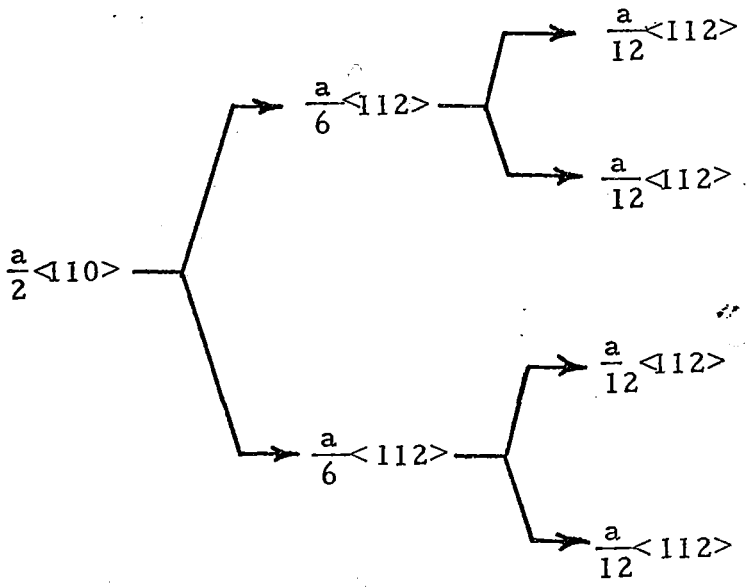

Large arrows in Fig. 14 indicate the sequence of formation, while smaller arrows point out intrinsic stacking faults in the austenite, and the formation of regular defects. Very small arrows in the illustration of martensite formation indicate the movement of $\frac{a}{12}\langle 112\rangle$ quarter dislocations. Two quarter dislocations or half Shockley partials in effect form a bcc fault by propogating in the same direction. Thus, a Shockley partial a/6 [112] dissociates into two half partials, a/12 [112] and a/12 [112]. The equilibrium width of this bcc fault is independent of the direction of an applied stress since the two half partials have the same slip direction. The austenite grain surface in the initial illustration can be imagined as the (110) surface with the horizontal and vertical directions essentially characterized by $[1\bar{1}2]$ and $[\bar{1}11]$ respectively. The normal surface layering sequence is shown as A, B, C illustrated as indicated. The path mechanism normally followed for shock-loaded

stainless steel and brass is $\gamma \rightarrow \gamma(F) \rightarrow \gamma(T) + \gamma(\varepsilon)$; and $\gamma(\varepsilon) \rightarrow (\alpha')$ for cold-rolled stainless steel. It is possible in some cases for the sequence $\gamma \rightarrow \gamma(F) \rightarrow \gamma(\varepsilon) \rightarrow \gamma(T) \rightarrow \gamma(\alpha')$ to occur. We observe that the α' transformation mechanism is probably one of nucleation at the configurations of Shockley partials as shown in the ε-phase schematic of Fig.14. However, Kelly[26] has pointed out that the order of formation of martensite or epsilon phase cannot be determined from a metallographic or crystallographic analysis. It is also observed that equally likely sites, in fact identical sites for α' formation, are contained in the twin boundaries shown in the schematic diagram of $\gamma(T)$ formation in Fig.14. Thus, under certain conditions, it would not be unlikely to find martensite (α or α') formed from twinned material, or twinning accommodated in the martensite. The transition from α to α' (bct $\rightarrow$bcc) is also to be recognized as an accommodation process involving slight shifting of the atom positions in the transformed lattice.

IV) CONCLUSIONS

On the basis of the above results, it is concluded that:

(1) The primary mode of deformation as a result of explosive shock loading in 304 stainless steel is the formation of twin-faults, while in 70/30 brass it appears to be predominantly planar dislocation arrays and twin-faults with a concomitant high dislocation density.

(2) The primary mode of deformation as a result of cold reduction of 70/30 brass and 304 stainless steel is the formation of coplanar dislocation arrays in brass; and stacking-fault bundles and (ε-martensite) α'-martensite in stainless steel.

(3) The residual defect structure in brass and stainless steel influences their mechanical properties. A high correlation is observed to exist between mechanical properties residual defect substructure.

(4) The residual twin-fault and planar dislocation structures introduced in shock-loaded and cold-rolled brass and stainless steel do not produce discontinuous yielding effects, but do strengthen the matrix by causing effective barriers to dislocation motion as determined by stress relaxation in the pre-yield region of the stress-strain curves for stainless steel.

(5) Martensite, occurring as a defect substructure in cold-rolled stainless steel, produces residual mechanical properties characterized by discontinuous yielding as a result of dislocation pinning and unpinning at interfacially segregated carbon atoms.

(6) Stacking faults and twin-faults in a deformed matrix are functionally identical to a grain refinement, and act as effective barriers to dislocation motion. The impedance to dislocation motion increases with increasing volume density of twin-faults.

(7) The formation of planar arrays of dislocations, stacking-faults, hcp-phase bundles, twins or twin-faults, and martensite (bcc phase) in low stacking-fault energy materials can be described, for the most part, as the propagation and interaction of partial dislocations.

ACKNOWLEDGEMENT

This research was supported in part by the U. S. Naval Weapons Laboratory Foundational Research Program, and was performed, for the most part, while one of (L. E. M.) was a consultant to the Research Division, U. S. Naval Weapons Laboratory, Dahlgren, Virginia. Final portions of the work were supported in part by a USC Joint Services Electronics Grant, AFOSR-69-1622, and NASA Multidisciplinary Research Grant No. NGL-50-018-044. Finally, the authors are especially grateful for the criticisms and suggestions made by several unknown reviewers.

REFERENCES

1. C. S. Smith, Trans. Met. Soc. AIME, 1958, Vol. 212, p. 574.
2. G. E. Dieter, in Strengthening Mechanisms in Solids, ASM, Metals Park, Ohio, 1962.
3. E. G. Zukas, Metals Engr. Quart., 1966, Vol. 6, p. 1.
4. R. L. Nolder and G. Thomas, Acta Met., 1964, Vol. 12, p. 227.
5. O. Johari and G. Thomas, Acta Met., 1964, Vol. 12, p. 1153.
6. M. F. Rose and F. I. Grace, Brit. J. Appl. Phys., 1967, Vol. 18, p. 671.
7. F. I. Grace, M. C. Inman and L. E. Murr, Brit. J. Appl. Phys., 1968, Vol. 1, p. 1473.
8. L. E. Murr, Appl. Matls. Res., 1964, Vol. 3, p. 153.
9. M. C. Inman, L. E. Murr, and M. F. Rose, Adv. Electron Metal (ASTM), 1966, STP. 396, p. 39.
10. P. R. Thornton and P. B. Hirsch, Phil. Mag., 1958, Vol. 3, p. 738.
11. S. R. Bodner, Mater. Sci. Engr., 1967, Vol. 2, p. 213.
12. P. Feltham, Phil. Mag., 1961, Vol. 6, p. 259.
13. G. A. Sargent and B. J. Shaw, Acta Met., 1966, Vol. 14, p. 909.
14. A. Art, R. Gevers and S. Amelinckx, Phys. Stat. Sol., 1963, Vol. 3, p. 697.
15. J. Van Landuyt, R. Gevers and S. Amelinckx, Phys. Stat. Sol., 1966 Vol. 18, p. 363.
16. A. S. Appleton and J. S. Waddington, Phil. Mag., 1965, Vol. 12, p. 273.
17. L. E. Murr and J. V. Foltz, J. Appl. Phys., in the press.

18. M. F. Rose and T. L. Berger, Phil. Mag., 1968, Vol. 17, p. 1121.

19. F. I. Grace, Ph.D. Dissertation, Pennsylvania State University, University Park, Pennsylvania, 1967.

20. L. E. Murr and F. I. Grace, Exp. Mech., 1969, Vol. 9, p. 145.

21. P. M. Kelly and J. Nutting, J. Iron St. Inst., 1961, Vol. 197, p. 199.

22. S. Dash and N. Brown, Acta Met., 1966, Vol. 14, p. 595.

23. R. Lagneborg, Acta Met., 1964, Vol. 12, p. 823.

24. J. A. Venables, Phil. Mag., 1961, Vol. 6, p. 379.

25. J. B. Cohen and J. Weertman, Acta Met., 1963, Vol. 11, p. 996.

26. P. M. Kelly, Acta Met., 1965, Vol. 13, p. 635.

Table 1. Sample Composition (weight per cent)

Sample	Fe	Ni	Cr	Cu	Zn	Mn	Si	C	balance
304 Stainless steel	70.39	9.52	18.43	0.14	---	1.05	0.42	0.06	---
70/30 Brass	---	---	---	69.59	30.39	---	---	---	0.02

Table 2. Residual Properties of Shock-Loaded 70/30 Brass

Shock Pressure (Kilobars)	Twin-Fault Density (Volume Per Cent)	Dislocation Density (10^{10} cm^{-2})	Vickers Micro-hardness (200 gm load)
0	0	*	161
120	5	0.1	220
150	9	0.6	243
235	27	2.1	301
345	33	3.8	320
425	44	6.0	341

*Initial dislocation density was computed to be $\sim 10^{6}$ cm^{-2}.

Table 3. Residual Properties of Cold-Rolled 70/30 Brass

Cold Reduction (Per Cent)	Twin-Fault Density (Volume Per Cent)	Dislocation Density (10^{10} cm^{-2})	Vickers Micro-hardness (200 gm load)
0	---	*	60
15	---	0.9	130
30	---	1.7	158
45	---	4.4	193
60	---	6.5	209
75	1	---	213

*Initial dislocation density was computed to be $\sim 10^{6}$ cm^{-2}.

Table 4. Residual Properties of Shock-Loaded 304 Stainless Steel

Shock Pressure (Kilobars)	Twin-Fault Density (Volume Per Cent)	Dislocation Density (10^{10} cm^{-2})	Vickers Micro-hardness (200 gm load)
0	0	*	161
120	5	0.1	220
150	9	0.6	243
235	27	2.1	301
345	33	3.8	320
425	44	6.0	341

*Initial dislocation density was computed to be 8×10^{5} cm^{-2}.

Table 5. Residual Properties of Cold-Rolled 304 Stainless Steel

Cold Reduction (Per Cent)	Martensite (α') Density (Volume Per Cent)	Dislocation Density (10^{10} cm^{-2})	Vickers Micro-hardness (200 gm load)
0	0	*	161
5	1	0.1	221
15	5	0.9	300
25	8	5.8	355
35	20	---	381
45	45	---	418

*Initial dislocation density was computed to be 8×10^{5} cm^{-2}.

Table 6. Activation Volume, V_A, and Dislocation Velocity Stress Dependence Parameter, m, for Deformed Stainless Steel from Room Temperature Stress Relaxation Data

Deformation	σ_o (Kpsi)*	V_A / b^3	m
0 (undeformed)	40, 60	33, 29	98, 100
150 Kb	75	33	141
235 Kb	65	41	173
425 Kb	90	64	329
25% C. R.	65	31	116
45% C. R.	80	60	276

* 1 Kpsi = 0.7 Kg/mm^2

FIGURE CAPTIONS

Fig. 1. Shock-loaded 70/30 brass showing planar dislocation arrays at 50 Kb(a) and 100 kilobars (b).

Fig. 2. Shock-loaded 70/30 brass showing (a) stacking faults after 200 kilobars shock pressure, and (b) dense twin-fault structures after shock loading to 400 kilobars pressure.

Fig. 3. Stress-elongation curves for shock-loaded brass. ($T = 300^{\circ}K$; $\dot{\epsilon} = 2.7 \times 10^{-3}\ sec^{-1}$).

Fig. 4. Dislocation substructures in 70/30 brass cold-rolled 15% (a) and 30% (b).

Fig. 5. Dislocation substructures in brass cold-rolled 45% (a) and 75% (b). The onset of twinning was observed at 75% reduction in thickness probably as a relief mechanism for the accommodation of plastic deformation.

Fig. 6. Stress-elongation curves for cold-rolled brass. ($T=300^{\circ}K$; $\dot{\epsilon} = 2.7 \times 10^{-3}\ sec^{-1}$).

Fig. 7. Shock-loaded 304 stainless steel showing typical stacking-fault structures in stainless steel shock-loaded to 120 kilobars (a), and well defined twin-fault structures following shock-loading at 235 Kb(b).

Fig. 8. Stress-elongation curves for shock-loaded stainless steel. ($T = 300^{\circ}K$; $\dot{\epsilon} = 2.7 \times 10^{-3}\ sec^{-1}$).

Fig. 9. Cold-rolled 304 stainless steel substructures showing stacking-faults following 5% reduction (a) and ϵ-phase bundles and stacking fault bundles following cold reduction of 15% (b).

Fig. 10. Martensite phase (α'-bcc) in cold-rolled type 304 stainless steel after reduction by 25% (a), and 35% (b).

Fig. 11. Stress-elongation curves for cold-rolled stainless steel ($T = 300^{\circ}K$; $\dot{\varepsilon} = 2.7 \times 10^{-3}$ sec^{-1}).

Fig. 12. Typical stress relaxation curves for cold-rolled and shock-loaded stainless steel in the pre-yield region of the stress-elongation curves.

Fig. 13. Stress relaxation from similar stress stops in the pre-yield region of the stress-elongation curves for cold-rolled and shock-loaded stainless steel as a function of time at room temperature ($300^{\circ}K$).

Fig. 14. Schematic diagrams illustrating the formation and probable sequence of formation of accommodation substructures by the movement of partial dislocations.

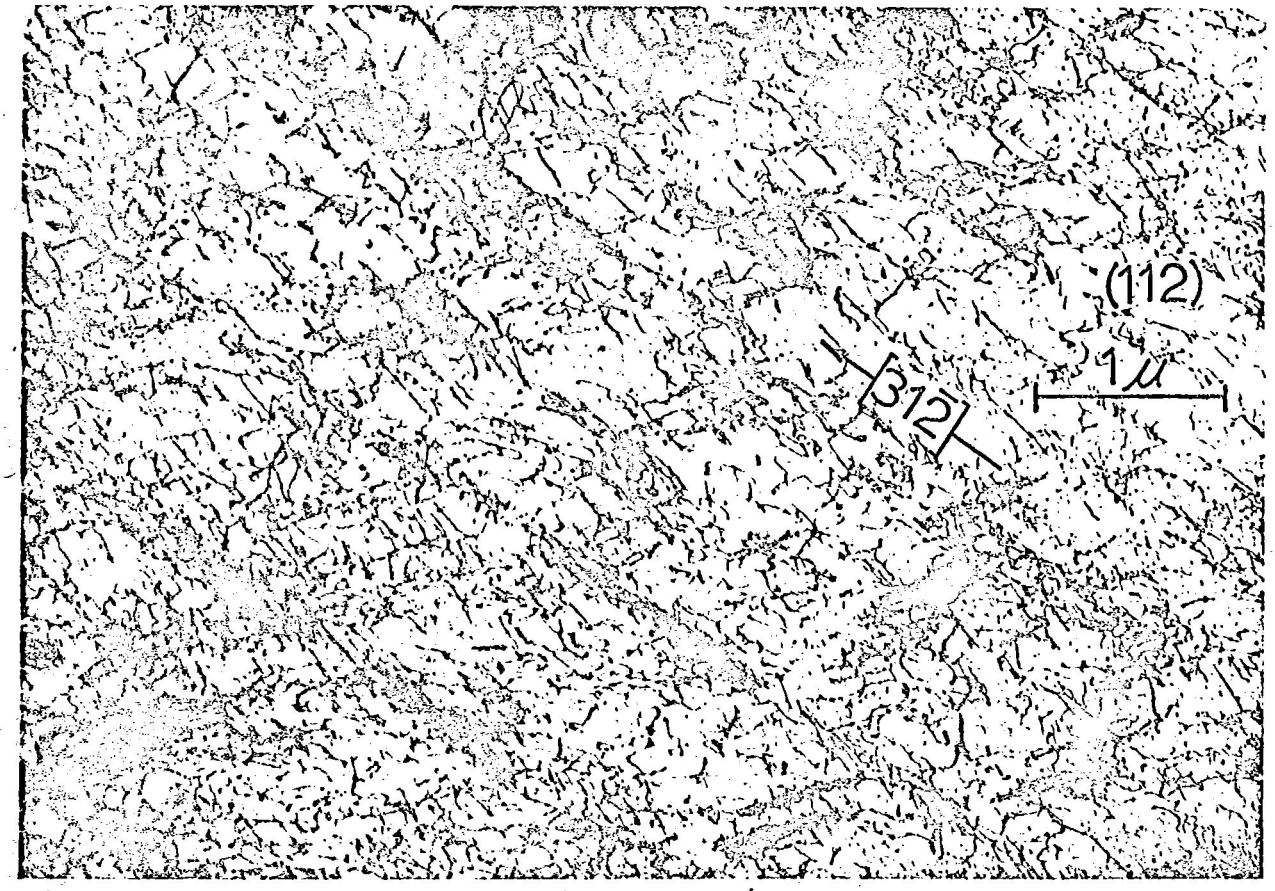

a

b

Mure & Grace FIG. 1

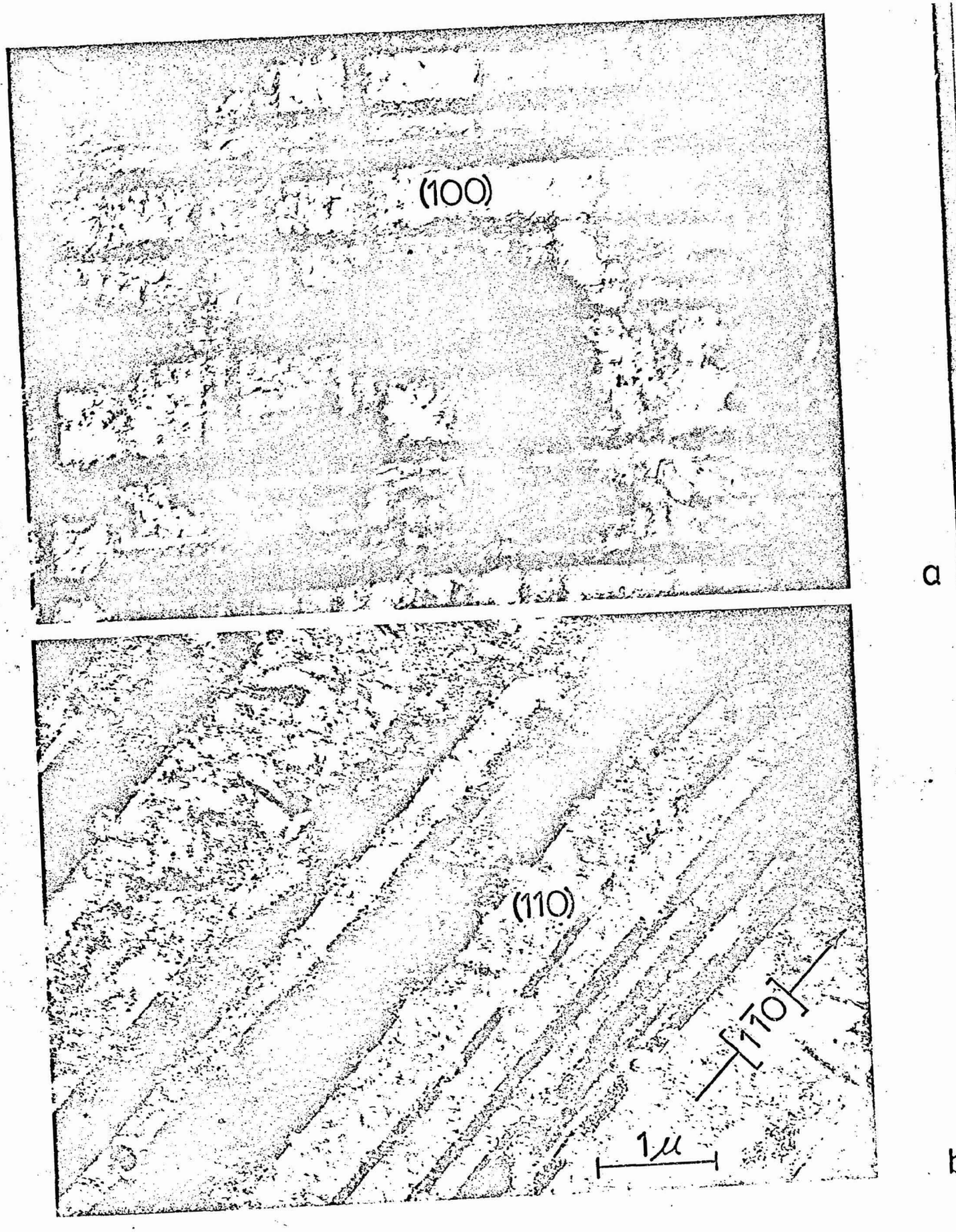

Miller & Grove FIG. 7

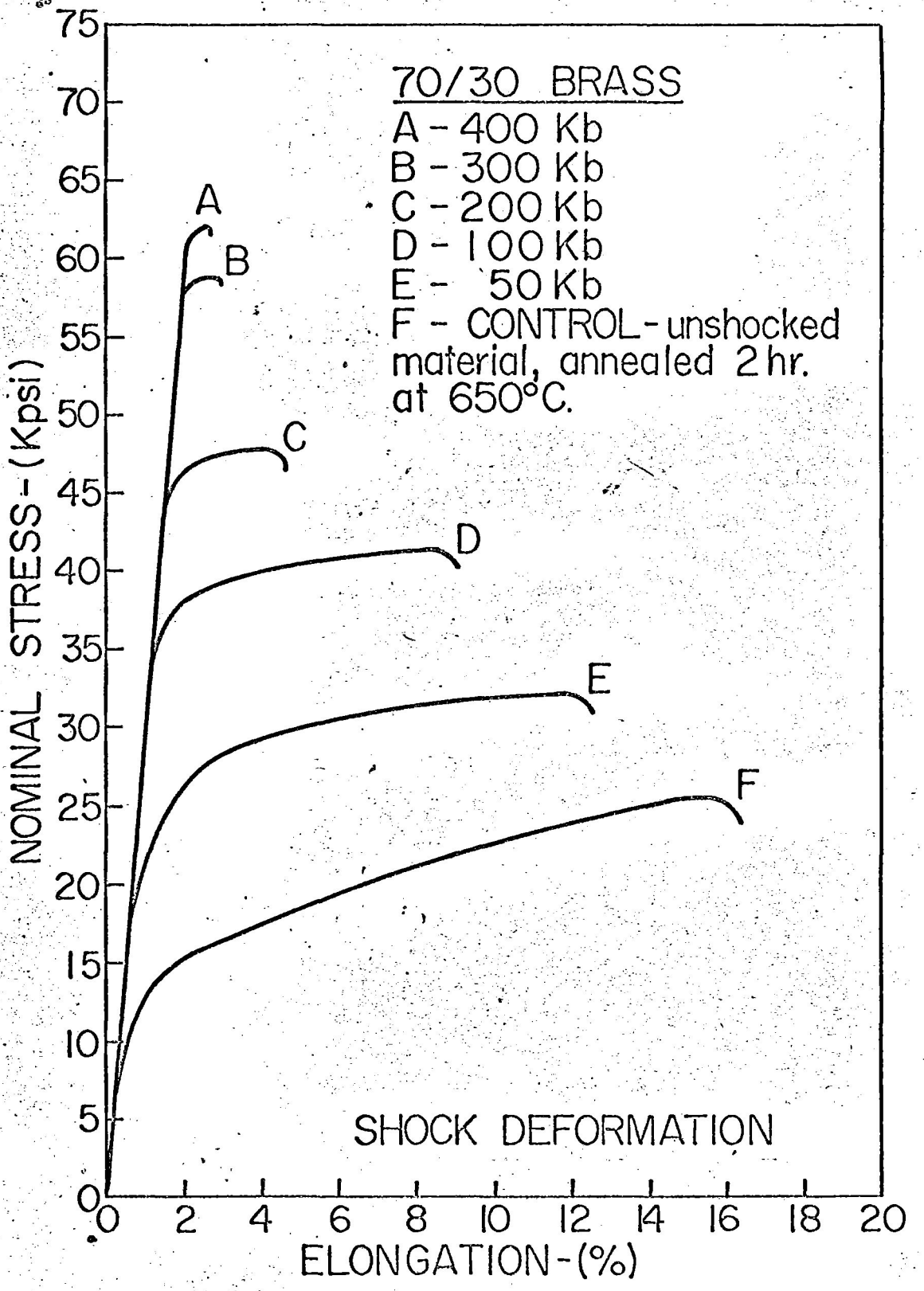

Marr & Greene FIG. 3

a

b

Muir & Grace FIG. 4

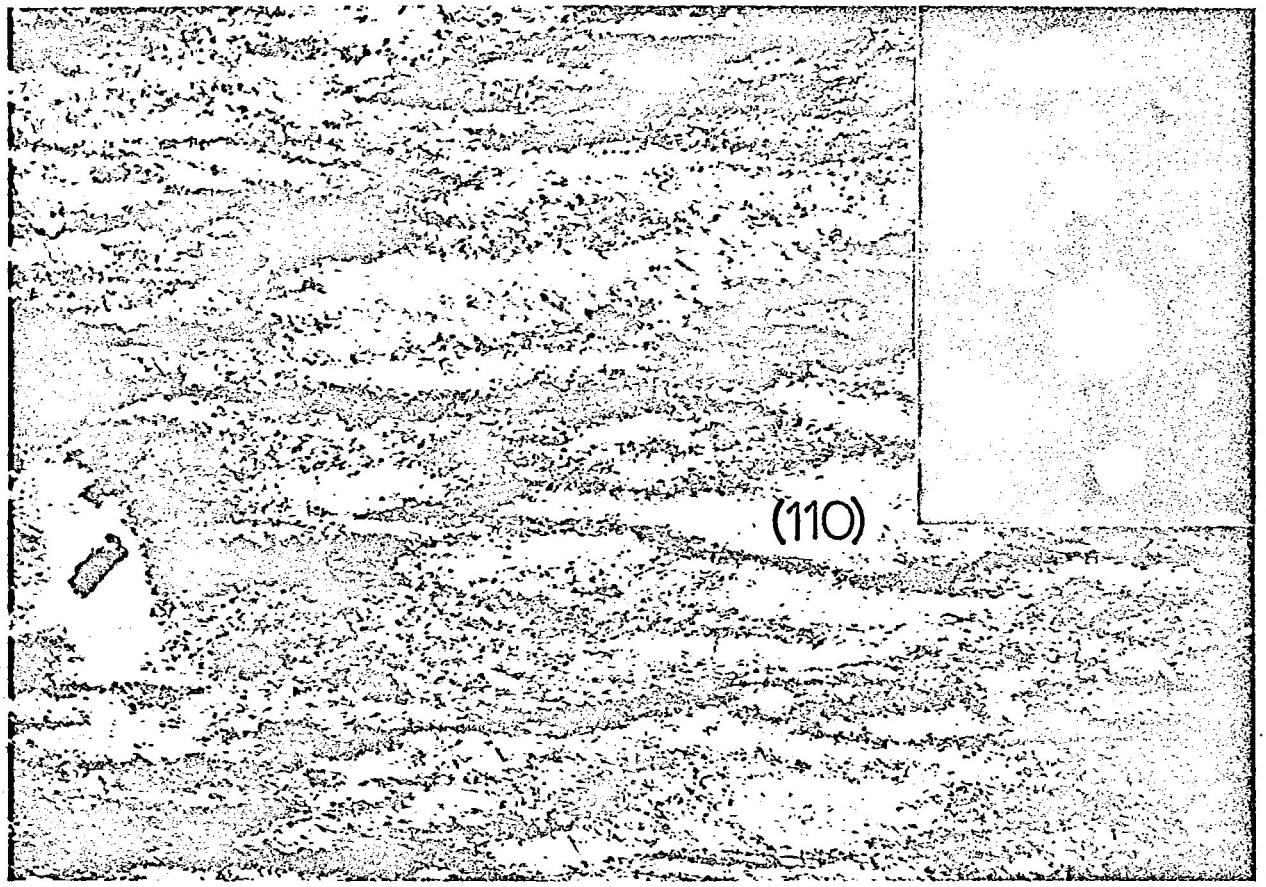

a

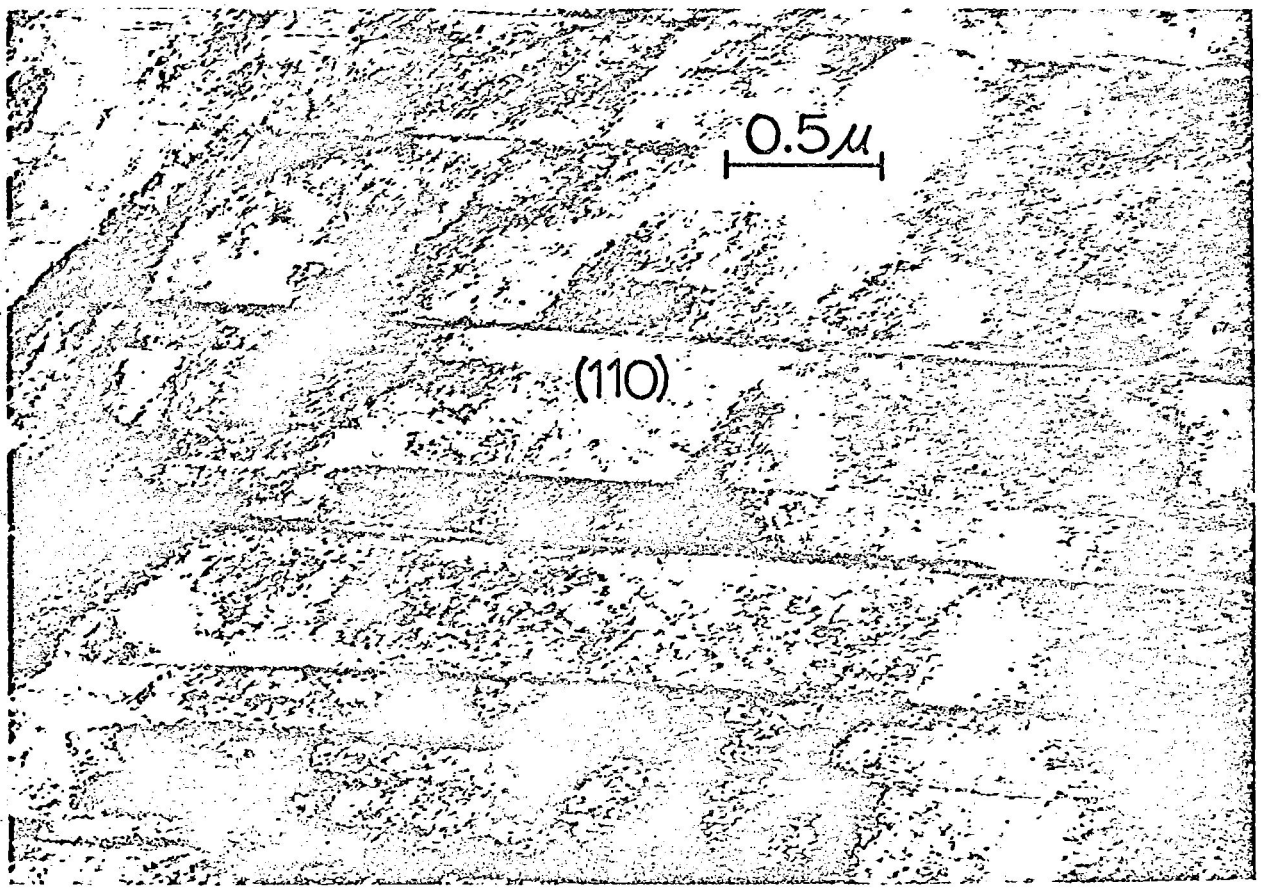

b

Muir & Grau FIG. 5

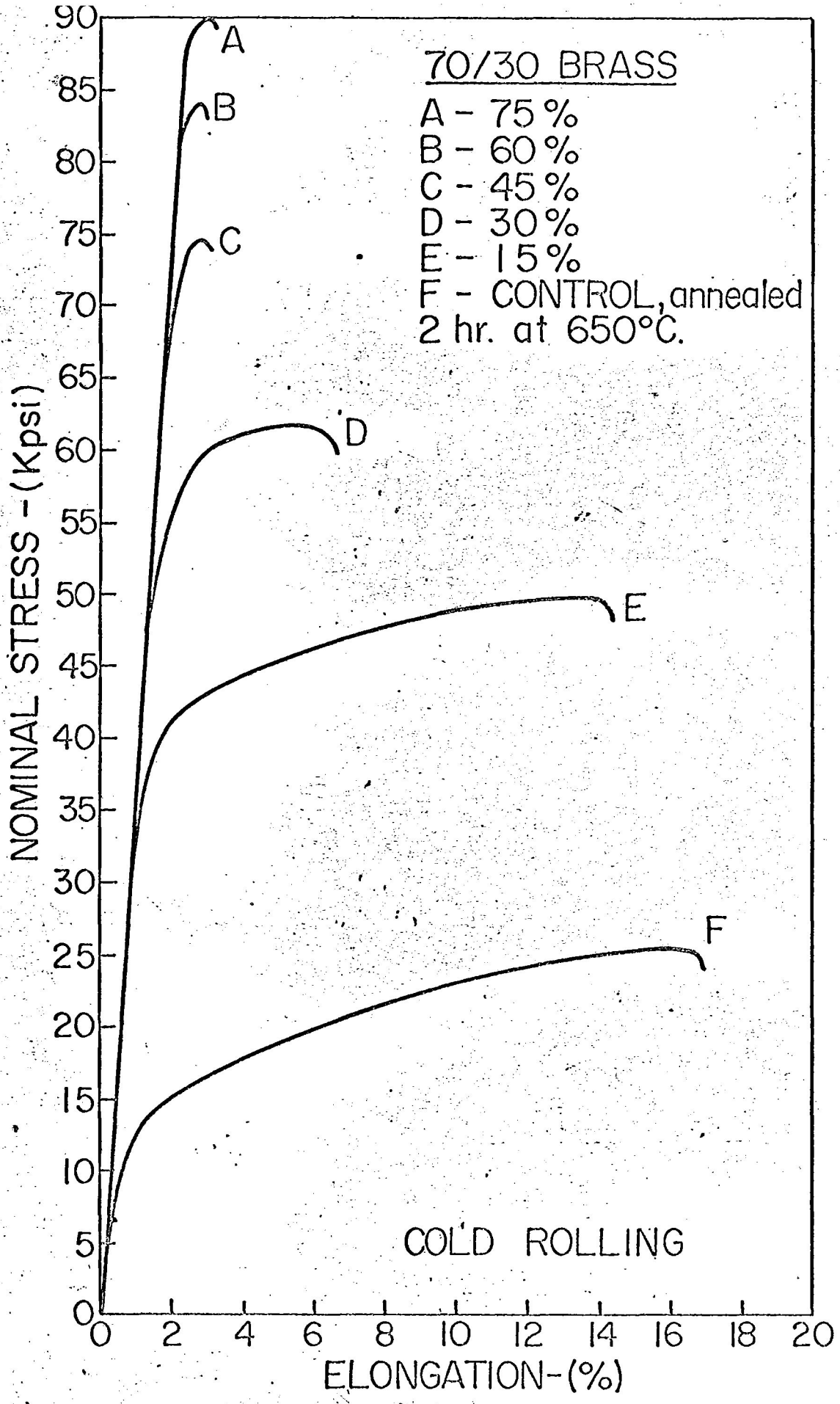

Murr & Grace FIG. 6

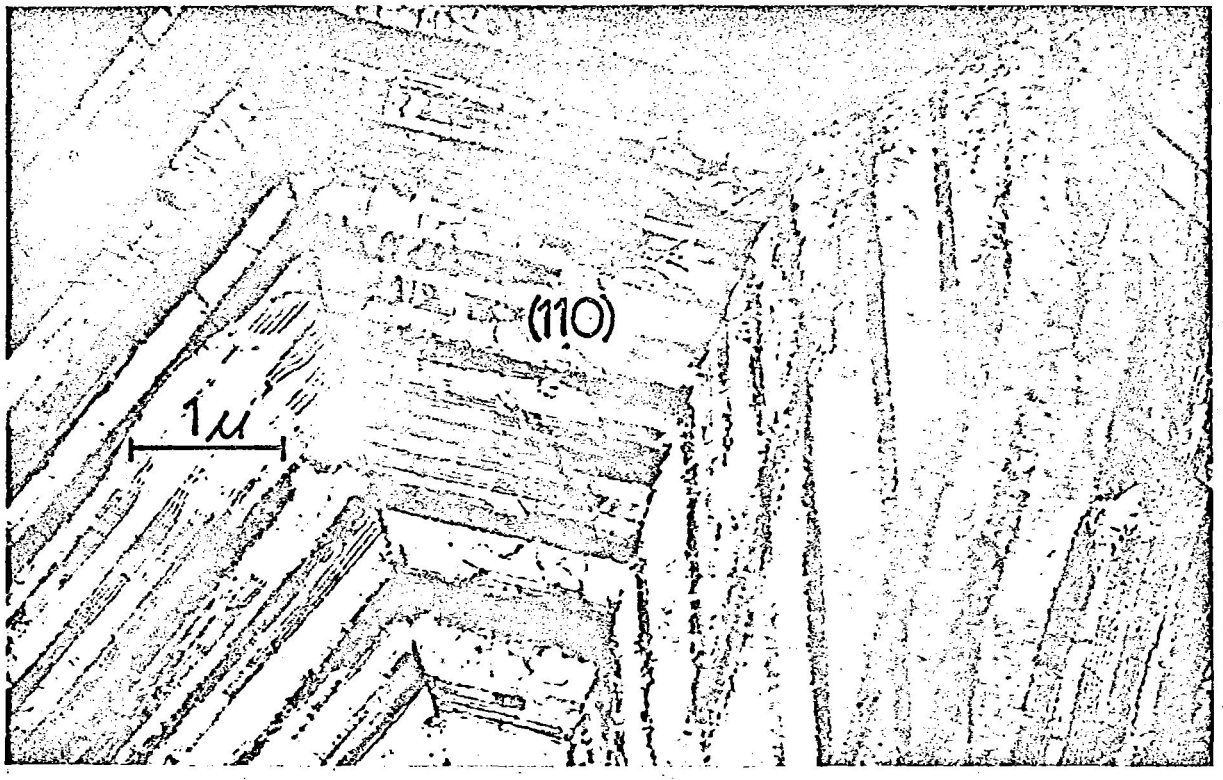

a

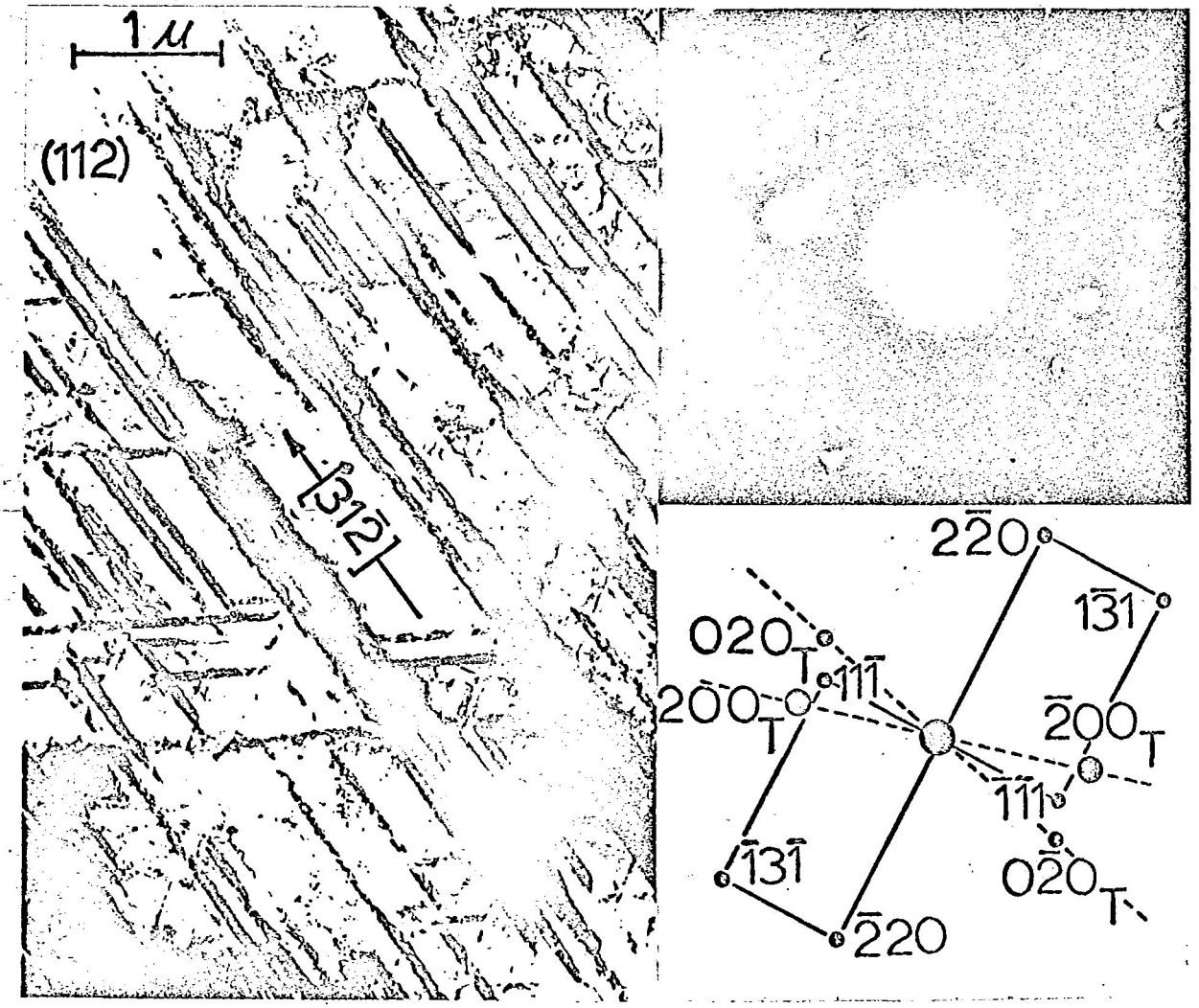

b

Murr & Grace Fig. 7

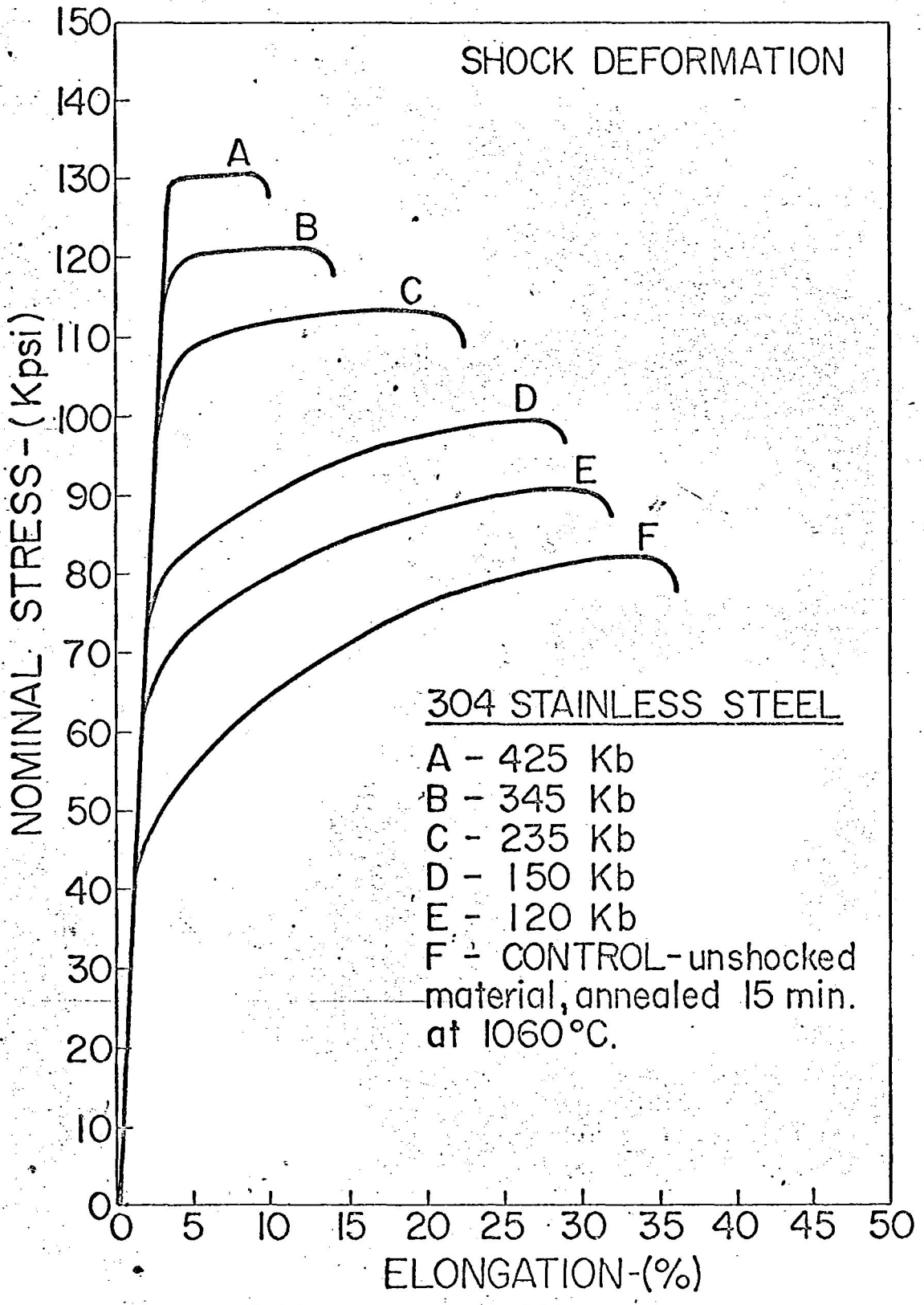

Heart of Girl FIG. 8

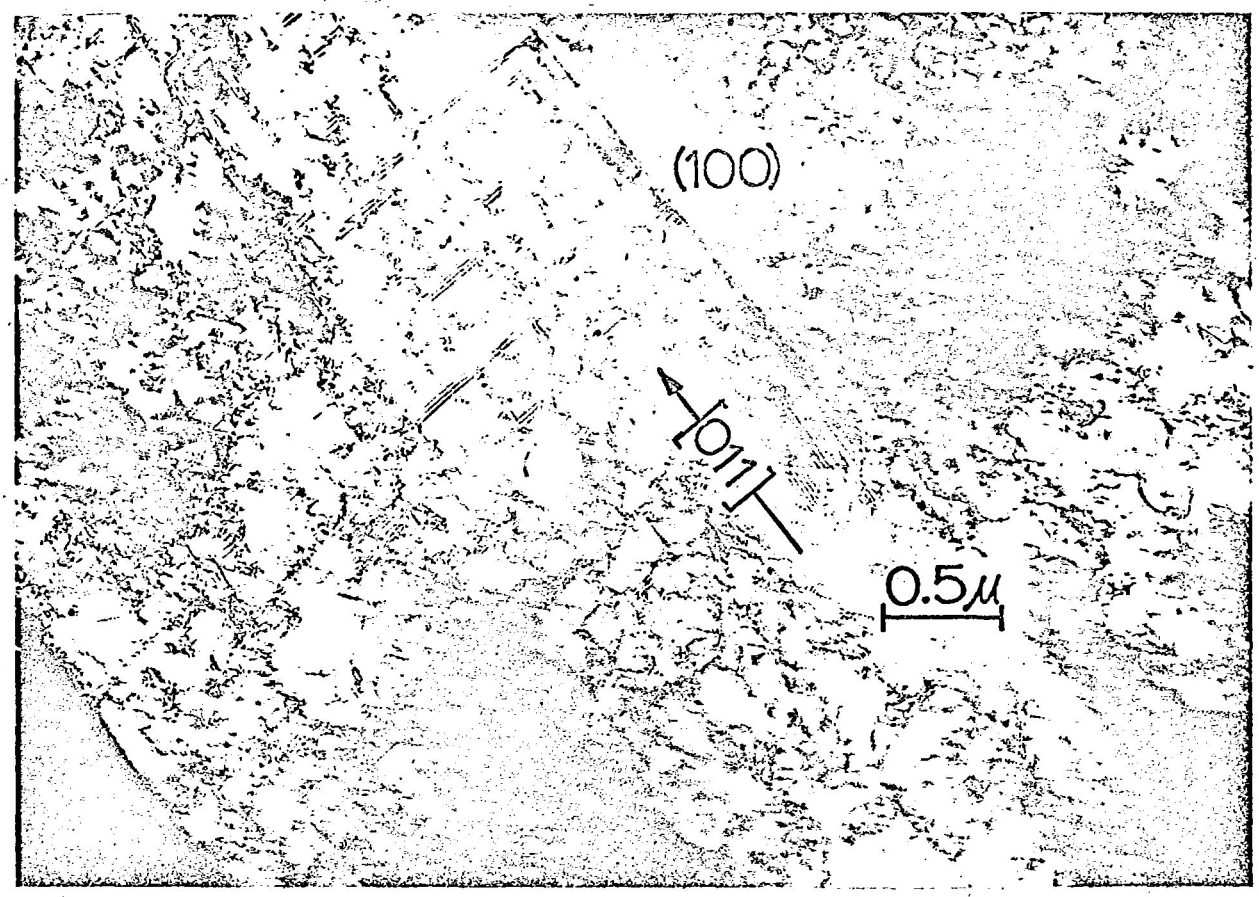

a

b

Murr & Grace FIG. 9

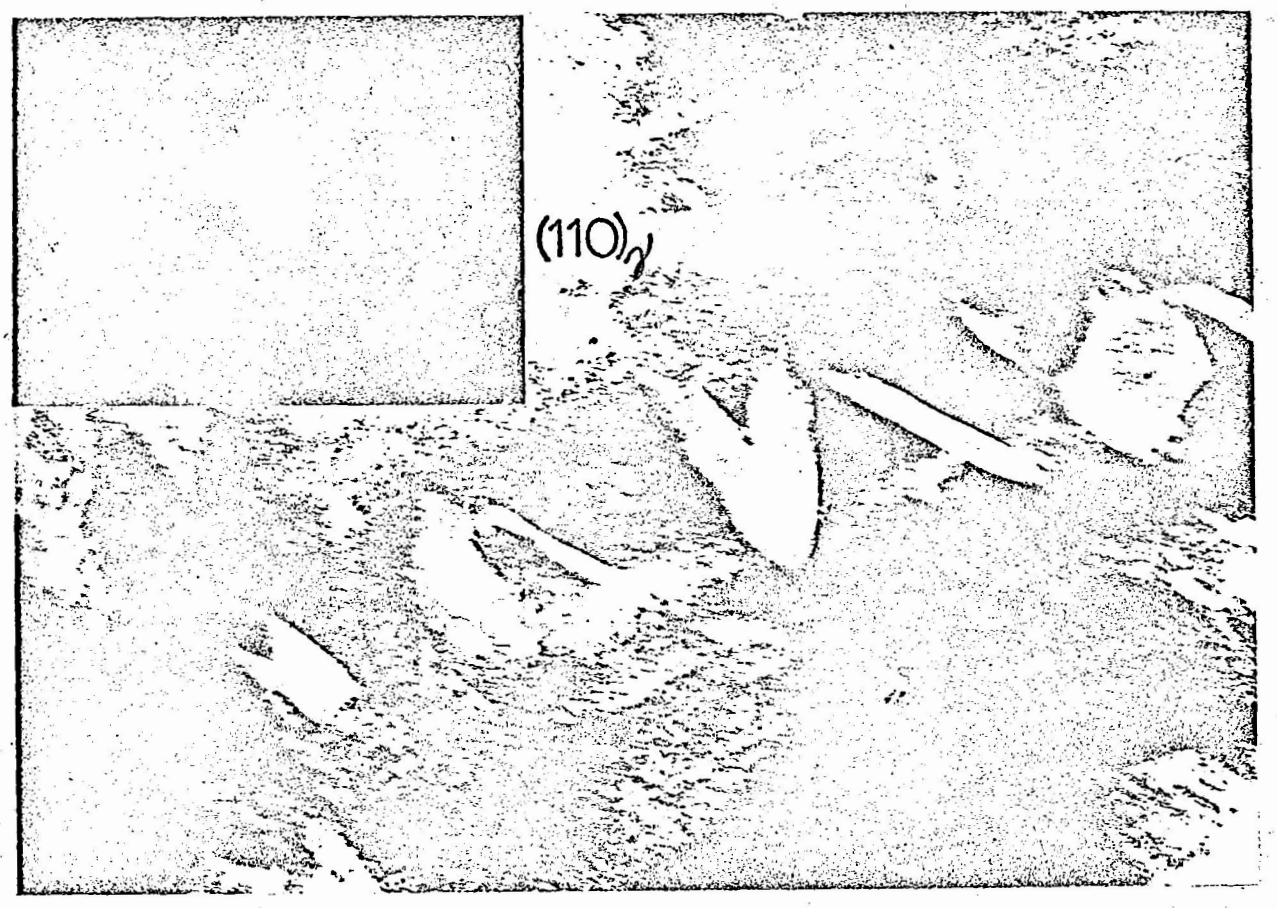

a

b

Murr & Grace FIG. 10

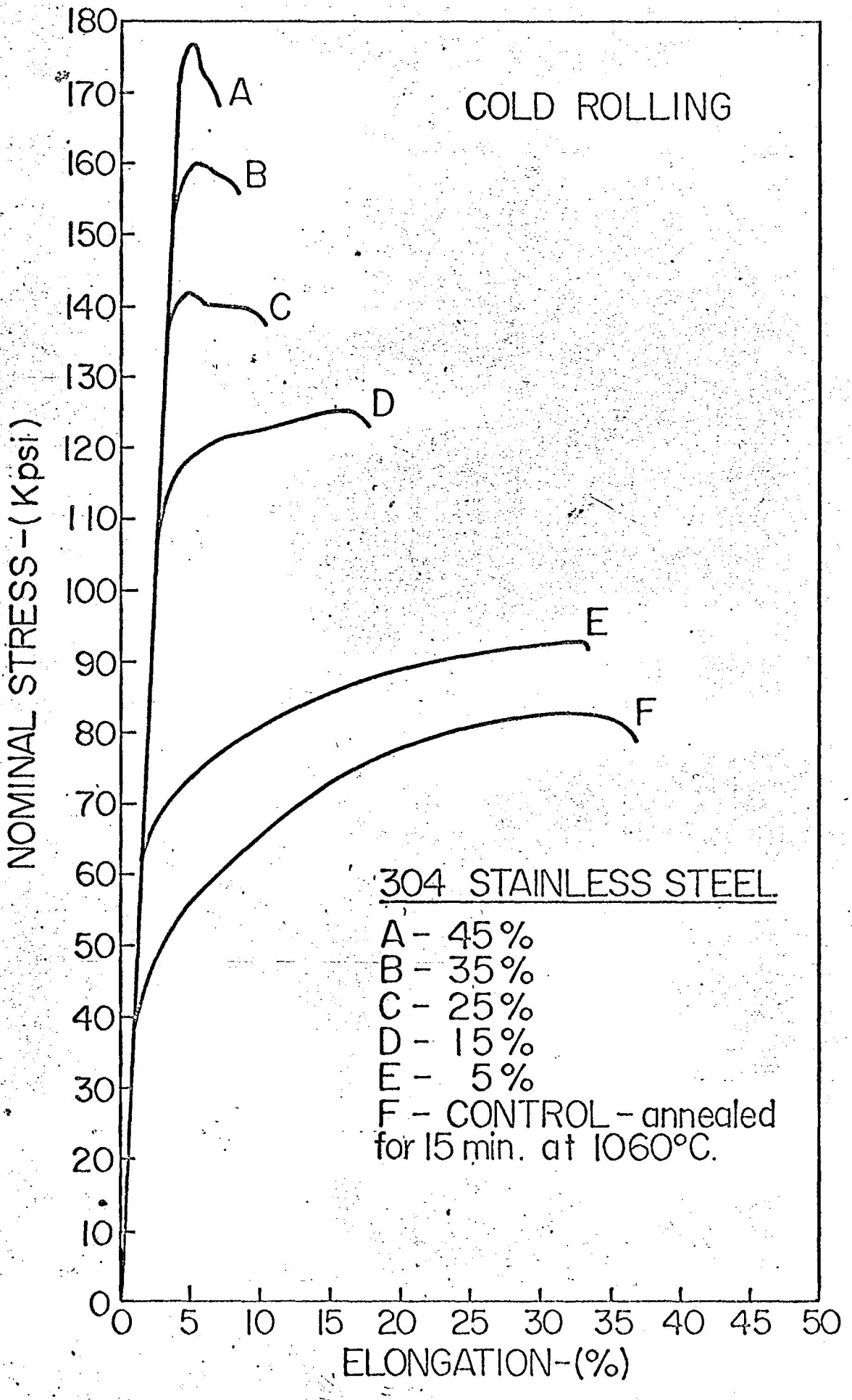

Murr & Grace FIG. 11

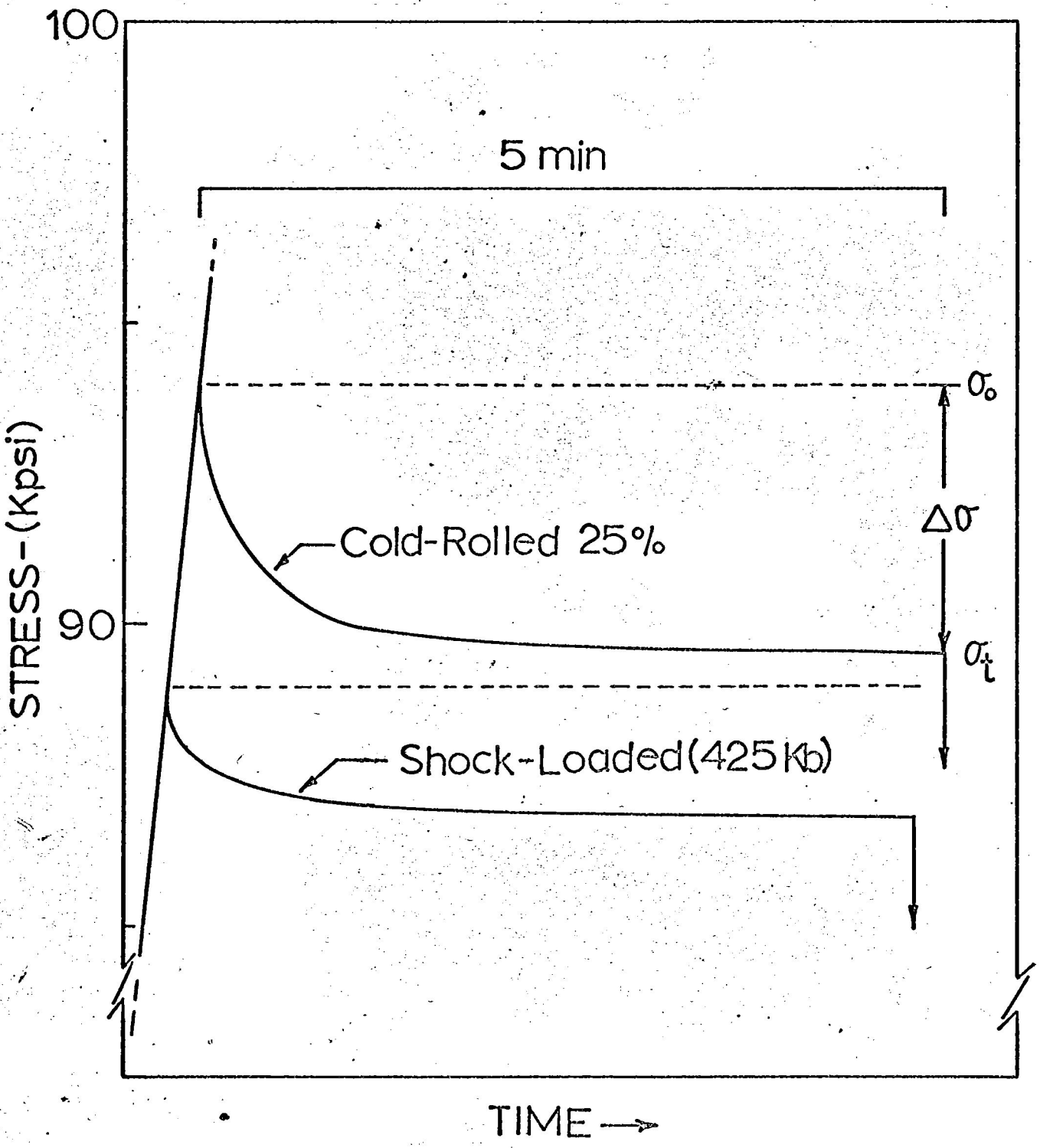
100
5 min
STRESS-(Kpsi)
90
σ_o
$\Delta\sigma$
σ_t
Cold-Rolled 25%
Shock-Loaded(425Kb)
TIME →

Fig. 12

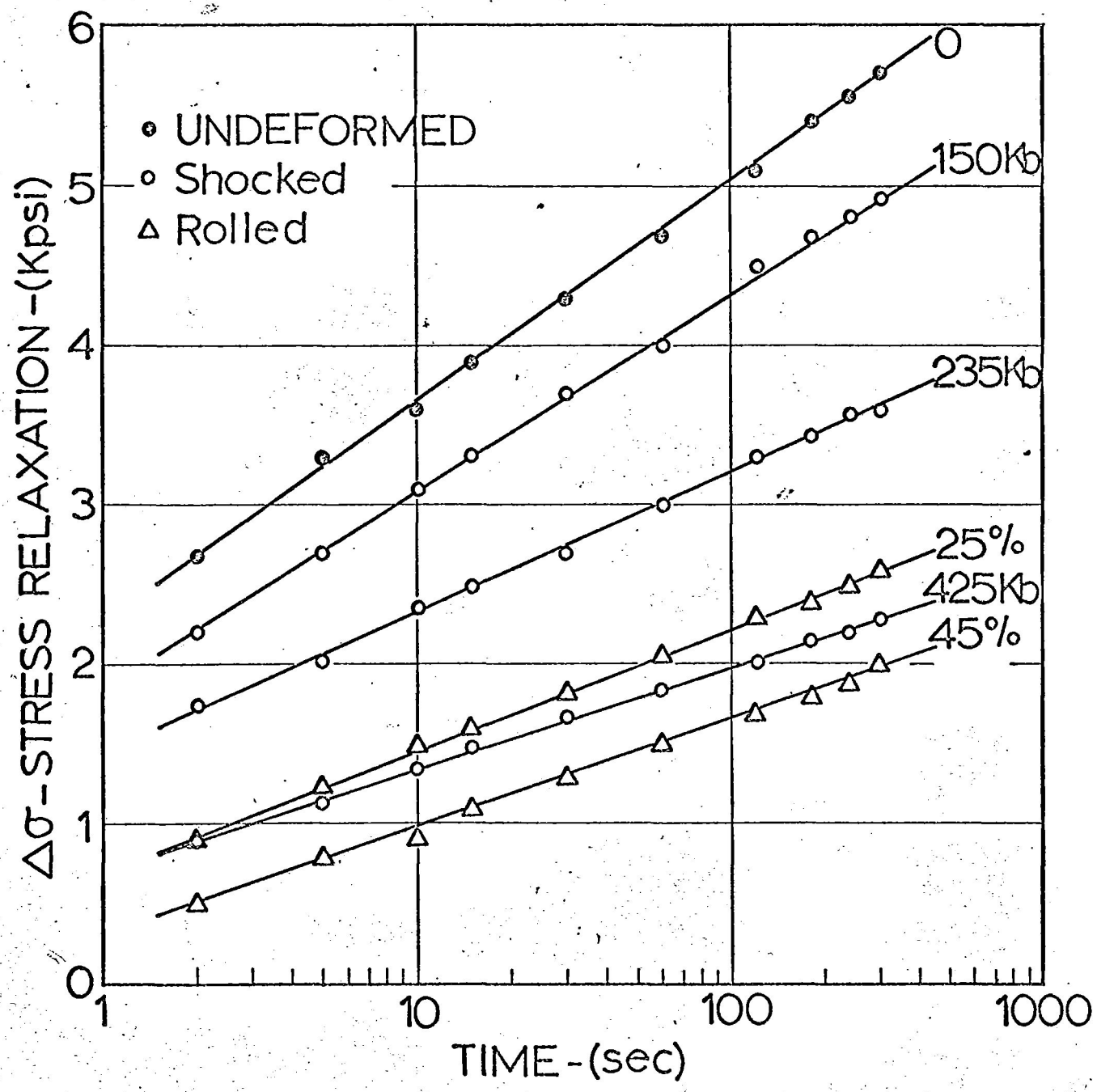
UNDEFORMED
Shocked
Rolled
0
150Kb
235Kb
25%
425Kb
45%
ΔσSTRESS RELAXATION-(Kpsi)
TIME-(sec)
0
1
2
3
4
5
6
1
10
100
1000

Fig. 13

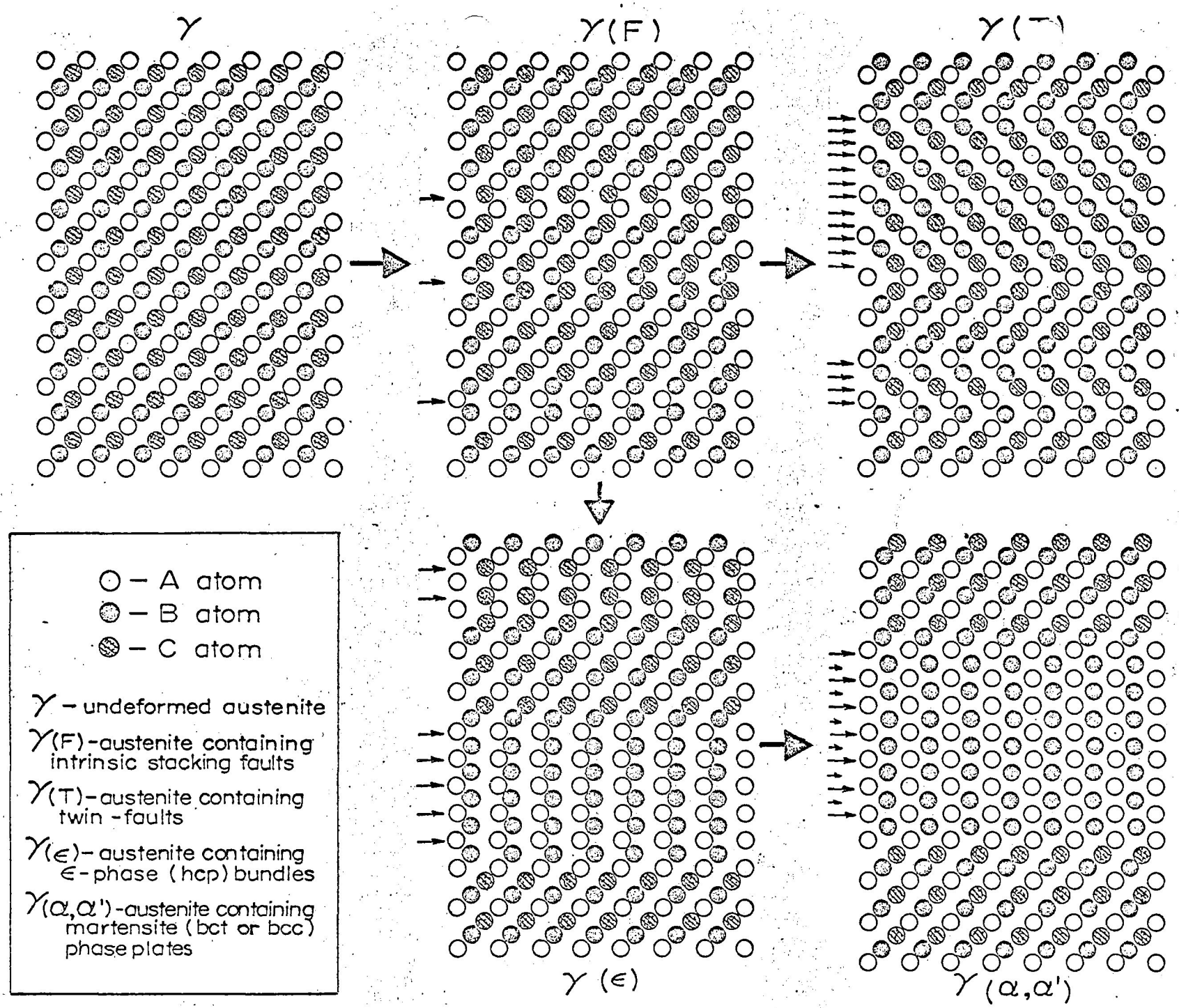
γ
γ(F)
γ(T)
○ – A atom
◎ – B atom
⊛ – C atom
γ – undeformed austenite
γ(F) – austenite containing intrinsic stacking faults
γ(T) – austenite containing twin – faults
γ(ϵ) – austenite containing ϵ – phase (hcp) bundles
γ(α,α') – austenite containing martensite (bct or bcc) phase plates
γ (ϵ)
γ (α,α')

Fig. 1-1